Heinrich Heine
Universität
Düsseldorf

Towards scalable active steering protocols for genuinely entangled state manifolds

Morales, Samuel; Egger, Reinhold; Pappalardi, Silvia

Article - Version of Record

Suggested Citation:
Morales, S., Pappalardi, S., & Egger, R. (2025). Towards scalable active steering protocols for genuinely entangled state manifolds. Physical Review Research, 7(2), Artikel 023170. https://doi.org/10.1103/physrevresearch.7.023170

Wissen, wo das Wissen ist.

UNIVERSITÄTS- UND LANDESBIBLIOTHEK DÜSSELDORF

This version is available at:

URN: https://nbn-resolving.org/urn:nbn:de:hbz:061-20261123-173309-9

Terms of Use:

This work is licensed under the Creative Commons Attribution 4.0 International License.

For more information see: https://creativecommons.org/licenses/by/4.0

Towards scalable active steering protocols for genuinely entangled state manifolds

Samuel Morales [1], Silvia Pappalardi [2], and Reinhold Egger [1]
[1] Institut für Theoretische Physik, Heinrich-Heine-Universität, D-40225 Düsseldorf, Germany
[2] Institut für Theoretische Physik, Universität zu Köln, Zülpicher Straße 77, 50937 Cologne, Germany

(Received 5 December 2024; accepted 22 April 2025; published 19 May 2025)

We introduce and analyze an active steering protocol designed to target multipartite entangled states. The protocol involves multiple qubits subjected to weak Bell-pair measurements with active feedback, where the feedback operations are optimized to maximize the quantum Fisher information. Our scheme efficiently reaches a genuinely entangled one-parameter state manifold. Numerical simulations for systems with up to 22 qubits suggest that the protocol is scalable and allows for high multipartite entanglement across the system.

DOI: 10.1103/PhysRevResearch.7.023170

I. INTRODUCTION

Active steering protocols have recently attracted a lot of attention [1–8]. By a sequence of (weak) measurements, followed by feedback operations determined by the measurement outcomes, one may prepare, stabilize, or manipulate arbitrary quantum states. (Following Ref. [9], we use "steering" as a proxy for "guiding" the system, which differs from "quantum steering" in quantum information theory [10].) Weak, i.e., almost noninvasive, measurements can be performed, for instance, by weakly coupling each system qubit to its own detector qubit, with projective measurements of the detector qubits [11]. The feedback policy is typically based on a cost function. Previous active steering protocols (see, e.g., Refs. [4,6,8]) have been limited to $N \leqslant 6$ system qubits, mainly because practically useful fidelity-based cost functions imply an exponential scaling of the algorithmic demands with the system size (N).

In this paper, we present an active steering protocol that utilizes the *quantum Fisher information* (QFI) [12] as a cost function. The QFI is a fundamental quantity in entanglement theory and quantum metrology, serving as a witness of multipartite entanglement [13–15] and a valuable resource for quantum-enhanced metrology [16–20]. Our QFI-based protocol allows one to efficiently reach a one-parameter manifold of genuinely entangled N-qubit states that maximize the QFI, namely Green-Hornberger-Zeilinger (GHZ) states [21],

$$|\Psi\rangle = \frac{1}{\sqrt{2}}(|000\cdots\rangle + e^{i\phi}|111\cdots\rangle), \tag{1}$$

with an angular parameter ϕ. (For a system qubit with Pauli matrices $\sigma^{x,y,z}$, we use $\sigma^z|0\rangle = |0\rangle$ and $\sigma^z|1\rangle = -|1\rangle$.) By using the QFI as a cost function, our protocol significantly accelerates the active steering process. It also allows one to target a specific state with a designated phase ϕ. Additionally, our findings suggest scalability with the system size N, offering promising potential for steering in larger quantum systems. We note that if one stops the protocol before the maximal value for the QFI has been reached, one may also access more general states beyond Eq. (1).

In contrast to the active steering protocol discussed below, which employs minimally invasive weak measurements, recent studies have explored measurement-based protocols with a single round of strong (projective) Bell measurements plus feedback; see Refs. [22–24] and references therein. Such protocols allow one to prepare a broad family of genuinely multipartite entangled states, including the GHZ state (1), in a very efficient manner. Depending on the experimental platform at hand, it is nonetheless of interest to study active steering protocols since one can, in principle, access arbitrary target states; see Ref. [6] and our discussion below. Moreover, active steering protocols offer the potential for generalization to quantum systems with continuous degrees of freedom.

In Sec. II, we formulate the active steering protocol in a platform-independent manner. Weak measurements and the associated quantum feedback effects have by now become standard experimental tools that are employed in various platforms; see, e.g., Refs. [25–33]. They allow for high-precision measurements, and an application of these techniques to our protocol could be very promising. Moreover, as shown recently in Ref. [8] for one or two system qubits, by including amplitude damping and dephasing in the stochastic master equation, active steering schemes of the type considered below are expected to be robust against the presence of error channels with sufficiently weak error rates. In fact, Ref. [8] established the existence of a finite threshold error rate, and as long as the error rate stays below the threshold, errors can be corrected "on the fly" by the protocol. Although numerical simulations of the present version of our protocol including error channels are computationally prohibitively expensive for large N because one has to simulate the time evolution of mixed states, the fact that the error threshold rate is almost identical for $N = 1$ and $N = 2$ [8] suggests that a finite error threshold will persist at least for moderate values of N. If the

Published by the American Physical Society under the terms of the Creative Commons Attribution 4.0 International license. Further distribution of this work must maintain attribution to the author(s) and the published article's title, journal citation, and DOI.

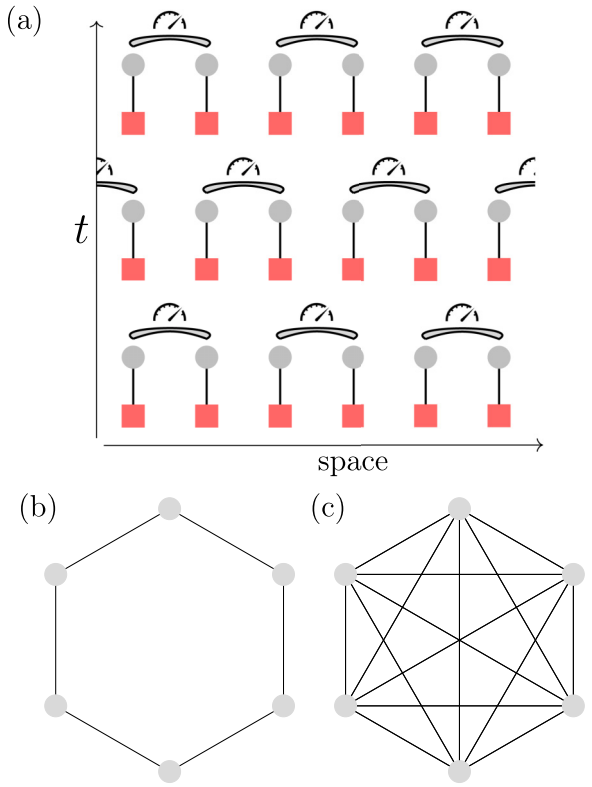


FIG. 1. Schematic time evolution of the active steering protocol. (a) We show three time steps for $N = 6$ system qubits (red squares) coupled by steering operators H_n (straight vertical lines) to their own detector qubits (grey circles). The qubit chain has periodic boundary conditions. A possible scheme for the Bell measurements of neighboring detector qubit pairs in subsequent cycles is indicated. (b) We mainly consider the case of Bell measurements of nearest-neighbor detector qubit pairs. (c) In Fig. 5 below, we also study the case where arbitrary detector qubit pairs can be subjected to Bell measurements (full connectivity).

system dynamics is described by a mixed state, one has to implement an unraveling procedure in practice for numerical stability. For large N, such approaches become exponentially costly in terms of computational demands. This restriction also applies when the detectors have nonideal measurement efficiency, since such effects are also captured by describing the system dynamics in terms of mixed states [34]. Furthermore, the QFI becomes more complicated for mixed states. For simplicity, we thus neglect external noise channels and nonideal measurement efficiencies, and study the error-free case with ideal measurements below. However, a modified implementation of our protocol that may allow us to circumvent these restrictions is discussed in Sec. IV.

Since weak measurements play a key role in our protocol, a physical realization with fast qubit readout is desirable, e.g., superconducting Andreev qubits with detector readout times of order 10 ns [35] could offer a good option [36]. We note that active steering protocols of a similar type have recently been experimentally implemented [37,38]. Our protocol assumes that the system is initialized at time $t = 0$ in a simple product state, say, $|\Psi(t = 0)\rangle = |000\cdots\rangle$, and that for a given measurement record, the state trajectory $|\Psi(t)\rangle$ can be stored and

TABLE I. Active steering protocol using the QFI as cost function. A classical computation of the measurement-averaged cost function change $\langle dF_Q(|\Psi\rangle, K)\rangle_{\rm ms}$ determines the optimal coupling $K = (K_n, K_{n+1})$ out of the coupling family $\mathcal{K} = \{K_n = (\alpha_n, \beta_n)|\alpha_n \in \{x, y, z\}; \beta_n \in \{x, z\}\}$ for qubit pair $(n, n+1)$. This choice is fed into the quantum computer as system-detector coupling. After unitary time evolution of duration δt, the detector is measured in the Bell basis $|\Phi_{\xi,\eta}\rangle_d$, where ξ and η correspond to the possible measurement outcomes. These are fed back into the classical computer to update and keep track of the system state.

choose $\|\Psi(0)\rangle = \|0\ldots0\rangle$ and $\mathcal{O}$		
Classical computer		Quantum computer
$\|\Psi(t)\rangle$		$\|\Psi(t)\rangle \to \|\Psi(t)\rangle \otimes \|00\rangle_d$
$\downarrow$		$\downarrow$
$\max_{K\in\mathcal{K}}\langle dF_Q(\|\Psi\rangle, K)\rangle_{\rm ms}$	$\xrightarrow{K\in\mathcal{K}}$	$e^{-i\delta t H_K}\|\Psi(t)\rangle \otimes \|00\rangle_d$
$\downarrow$		$\downarrow$
$\|\Psi(t+\delta t\|\xi,\eta)\rangle$	$\xleftarrow{(\xi,\eta)}$	${}_d\langle\Phi_{\xi,\eta}\|e^{-i\delta t H_K}\|00\rangle_d \times \|\Psi(t)\rangle$

updated on a classical computer for each time step of the quantum protocol. After introducing the protocol in Sec. II, we present numerical simulation results in Sec. III. We primarily focus on the GHZ state, but we also show how to prepare so-called Dicke states using this approach. In Sec. IV, we discuss several open issues and directions for future research. In particular, we outline how the state tracking requirement may be avoided in modified implementations of our protocol.

II. PROTOCOL AND QFI

We schematically illustrate the protocol in Fig. 1 and Table I. Each protocol step of time duration δt has two components, namely (i) unitary evolution of the coupled system and detector qubits under the chosen feedback Hamiltonian, followed by (ii) weak measurements of the system qubits via Bell-pair measurements of the detector qubits. Depending on the measurement outcomes, the feedback Hamiltonian for the next iteration step is then determined according to the decision making scheme discussed below.

We consider N system qubits described by Pauli matrices σ_n^α (with $\alpha = x, y, z$ and $n = 1, \ldots, N$), where each system qubit couples only to its own detector qubit described by Pauli matrices τ_n^β. We neither allow for direct couplings between different system qubits nor between different detector qubits, while the Hamiltonian H_n ("steering operator") for the nth system-detector qubit pair can be selected from the set of Pauli gates,

$$H_n = J\sigma_n^{\alpha_n}\tau_n^{\beta_n}, \tag{2}$$

with $\alpha_n \in \{x, y, z\}$ and $\beta_n \in \{x, z\}$. For simplicity, we assume a fixed coupling J, where we put $J = +1$ in what follows, and degenerate zero-energy states for all uncoupled qubits. The steering parameters $K_n = (\alpha_n, \beta_n)$ are chosen according to a decision making scheme in every time step of the protocol as described below, with $[H_n, H_{n'}] = 0$ for arbitrary K_n and $K_{n'}$.

Table I illustrates the active steering protocol using Bell-state measurements on neighboring pairs [see Fig. 1(b)] of detector qubits. Later on, we also consider the case in Fig. 1(c)

where Bell measurements can be performed for arbitrarily chosen pair orderings (with a given pairing order determined from a uniform random distribution), but we focus on the nearest-neighbor case in what follows. For a given time step of the protocol, all non-overlapping pairs $(n, n+1)$ can be steered simultaneously; see Fig. 1(a). One can either choose an alternating sequence of pairings on subsequent time steps, as shown in Fig. 1(a), or simply assign the pairing order randomly. In our simulations, we found the second option to be more efficient. As explained below, the active decision making is performed on a classical computer using knowledge about the present state of the system.

Let us now describe the protocol in detail. We start at time $t = 0$ by initializing all system and detector qubits in $|0\rangle$ and $|0\rangle_d$ (the subscript d refers to detector qubit space), respectively, i.e., the system state is $|\Psi(t=0)\rangle = |000\cdots\rangle$. We then group the N qubits into neighboring pairs $(n, n+1)$, see Fig. 1, where all subsequent operations for different pairs commute and can thus be performed simultaneously. (For odd N, one "idle" qubit remains, whose location is chosen from a uniform random distribution.) Given the state $|\Psi(t)\rangle$, for active steering towards the GHZ state, we select the steering couplings for this pair, (K_n, K_{n+1}), such that the measurement-averaged expectation value of the QFI after a time step of duration δt is maximized.

For a pure N-qubit state $|\Psi\rangle$, the QFI is defined as [16–20]

$$F_Q = 4(\langle\Psi|\mathcal{O}^2|\Psi\rangle - \langle\Psi|\mathcal{O}|\Psi\rangle^2). \tag{3}$$

For collective observables $\mathcal{O} = \frac{1}{2}\sum_{n=1}^{N} O_n$, where O_n are local operators, the QFI can be used to probe the multipartite entanglement structure of the state $|\Psi\rangle$ [13–15]. If the QFI satisfies the inequality $F_Q > mN$, then at least $(m+1)$ parties of the system are entangled. Namely, $m \leqslant N$ represents the size of the biggest entangled block. The upper bound $F_Q \sim N^2$ corresponds to the so-called genuinely multipartite entanglement. In particular, the family of states that saturate the maximum value of multipartite entanglement is an arbitrary superposition of the eigenvectors of $\mathcal{O}$ with largest and smallest eigenvalues. For $\mathcal{O} = \frac{1}{2}\sum_{n=1}^{N}\sigma_n^z$, these correspond to the states defined in Eq. (1).

In our protocol, we parametrize $O_n = \mathbf{s}_n \cdot \boldsymbol{\sigma}_n$, with $\mathbf{s}_n = (s_n^x, s_n^y, s_n^z)$ an arbitrary unit vector and $\boldsymbol{\sigma}_n = (\sigma_n^x, \sigma_n^y, \sigma_n^z)$. Using the optimal choice for (K_n, K_{n+1}), discussed below after Eq. (6), one time-evolves the coupled system-plus-detector system for a time step δt. Next, a projective measurement of the detector qubit pair is done in its Bell-state basis $\{|\Phi_{\xi,\eta}\rangle_d\}$ [21], where $|\Phi_{\xi=0,\eta=\pm}\rangle_d = (|00\rangle_d \pm |11\rangle_d)/\sqrt{2}$ and $|\Phi_{\xi=1,\eta=\pm}\rangle_d = (|01\rangle_d \pm |10\rangle_d)/\sqrt{2}$. Symmetric $(\eta = +1)$ and antisymmetric $(\eta = -1)$ Bell states have even $(\xi = 0)$ or odd $(\xi = 1)$ parity, where "symmetry" refers to qubit exchange while even (odd) "parity" means that states are built from the basis $\{|00\rangle_d, |11\rangle_d\}$ ($\{|01\rangle_d, |10\rangle_d\}$). Such measurements can be implemented by commuting measurements of the Pauli operators $\tau_n^z\tau_{n+1}^z = \pm 1$ and $\tau_n^x\tau_{n+1}^x = \pm 1$. Finally, one reinitializes all detector qubits in the state $|0\rangle_d$ and iterates the protocol until convergence has been achieved. Since the initial detector state $|00\rangle_d$ (for each time step and each qubit pair) has even parity, measurement outcomes with odd parity $(\xi = 1)$ are referred to as quantum jumps. The above measurements realize entanglement swapping [39–46] and tend to increase entanglement in the system state $|\Psi(t)\rangle \to |\Psi(t+\delta t)\rangle$; see Ref. [6] for a detailed discussion.

In the weak-measurement limit $J\delta t \ll 1$ [11], the state change $|d\Psi\rangle = |\Psi(t+\delta t)\rangle - |\Psi\rangle$ with $|\Psi\rangle = |\Psi(t)\rangle$ for measurement outcome (ξ, η) is governed by a jump-type nonlinear stochastic Schrödinger equation (SSE) [30,34,47],

$$|d\Psi\rangle = \left[-i\delta t H_0 + \xi\left(\frac{c_\eta}{\sqrt{\langle c_\eta^\dagger c_\eta\rangle}} - 1\right) - \frac{\delta t}{2}(c_\eta^\dagger c_\eta - \langle c_\eta^\dagger c_\eta\rangle)\right] \times |\Psi\rangle, \tag{4}$$

where $H_0 = J\sum_{m=n,n+1}\delta_{\beta_m,z}\sigma_m^{\alpha_m}$ and $\langle c_\eta^\dagger c_\eta\rangle = \langle\Psi|c_\eta^\dagger c_\eta|\Psi\rangle$. The jump operators $c_{\eta=\pm}$ are given by

$$c_\eta = -iJ\sqrt{\delta t}\left(\eta\delta_{\beta_n,x}\sigma_n^{\alpha_n} + \delta_{\beta_{n+1},x}\sigma_{n+1}^{\alpha_{n+1}}\right), \tag{5}$$

where the outcome (ξ, η) has the *a priori* probability $p_{\xi,\eta} = \frac{1}{2}[\delta_{\xi,0} + (\delta_{\xi,1} - \delta_{\xi,0})\delta t\langle c_\eta^\dagger c_\eta\rangle]$. Averaging over the measurement outcomes after one time step, one arrives at the anticipated average change in QFI after the next time step,

$$\begin{aligned}\langle dF_Q\rangle_{\rm ms} &= \langle F_Q(t+\delta t)\rangle_{\rm ms} - F_Q(t)\\ &= 4(\mathrm{Tr}(\mathcal{O}^2\langle d\rho\rangle_{\rm ms}) - 2\mathrm{Tr}(\mathcal{O}\langle d\rho\rangle_{\rm ms})\mathrm{Tr}(\mathcal{O}\rho)\\ &\quad - \langle[\mathrm{Tr}(\mathcal{O}\,d\rho)]^2\rangle_{\rm ms})\end{aligned} \tag{6}$$

with $d\rho = |d\Psi\rangle\langle\Psi| + |\Psi\rangle\langle d\Psi| + |d\Psi\rangle\langle d\Psi|$ and $\rho = |\Psi\rangle\langle\Psi|$. (Here, $\langle A\rangle_{\rm ms}$ denotes a measurement average of the quantity A using the probabilities $p_{\xi,\eta}$.) We compute $\langle dF_Q\rangle_{\rm ms}$ for all possible steering parameters and then choose (K_n, K_{n+1}) such that $\langle dF_Q\rangle_{\rm ms}$ is maximized. We emphasize that (K_n, K_{n+1}) is determined separately for each qubit pair at a given time step. In our numerical simulations, the system state is propagated according to the SSE (4). In contrast to Ref. [6], the time evolution is not terminated once a certain threshold value for F_Q has been reached but the quantum state trajectory continues evolving according to the above protocol.

Let us provide some details on the calculation of $\langle dF_Q\rangle_{\rm ms}$. The classical computation of $\langle dF_Q(|\Psi\rangle, K)\rangle_{\rm ms}$ for $H_K = H_n + H_{n+1}$ with $K = (K_n, K_{n+1})$ is performed numerically in a Bloch tensor representation of the system state,

$$|\Psi\rangle\langle\Psi| = \frac{1}{2^N}\sum_{\mathcal{S}} R_{\mathcal{S}}\mathcal{S}, \quad R_{\mathcal{S}} = \langle\Psi|\mathcal{S}|\Psi\rangle, \tag{7}$$

with the Pauli string operator $\mathcal{S} = \sigma_1^{\mu_1}\sigma_2^{\mu_2}\cdots\sigma_N^{\mu_N}$ with $\mu_j \in \{0,1,2,3\}$. Using this representation to parametrize the observables, the average QFI change is obtained as

$$\begin{aligned}\langle dF_Q\rangle_{\rm ms} &= \sum_{n\neq m}\sum_{\alpha_i,\alpha_j} s_n^{\alpha_n}s_m^{\alpha_m}\langle dQ_{n,m}^{\alpha_n,\alpha_m}\rangle_{\rm ms} - 2\left(\sum_{n,\alpha_n} s_n^{\alpha_n}\langle dR_n^{\alpha_n}\rangle_{\rm ms}\right)\\ &\quad\times\left(\sum_{n,\alpha_n} s_n^{\alpha_n}R_n^{\alpha_n}\right) - 2\delta t\sum_{\eta}\frac{1}{\langle c_\eta^\dagger c_\eta\rangle}\\ &\quad\times\left(\sum_{n,\alpha_n} s_n^{\alpha_n}G_{\alpha_n}^{(\eta)}\right)^2,\end{aligned} \tag{8}$$

where we used the reduced single-qubit Bloch vectors $R_n^{\alpha_n} = \langle\Psi|\sigma_n^{\alpha_n}|\Psi\rangle$ and the two-qubit correlators $Q_{n,m}^{\alpha_n,\alpha_m} = \langle\Psi|\sigma_n^{\alpha_n}\sigma_m^{\alpha_m}|\Psi\rangle$. For explicit expressions for $\langle dR_n^{\alpha_n}\rangle_{\rm ms}$ and $\langle dQ_{n,m}^{\alpha_n,\alpha_m}\rangle_{\rm ms}$; see Eq. (27) in Ref. [6]. The second-order state change of the single qubit density matrices for $\xi = 1$ measurement outcomes is given by

$$G_{\mu_i}^{(\eta)} = -\sum_{m=n,n+1}\sum_{\alpha\neq\alpha_i}\Gamma_m\delta_{\beta_m,x}\delta_{\mu_i,\alpha}R_{\mu_i} + \eta\sqrt{\Gamma_n\Gamma_{n+1}}\delta_{\beta_n,x}\delta_{\beta_{n+1},x}(\mathcal{F}_{\mu_i} - Q_{n,n+1}R_{\mu_i}),$$

$$\mathcal{F}_{\mathcal{S}} = \frac{1}{2^{N+1}}\sum_{\mathcal{S}}{}' R'_{\mathcal{S}}\mathrm{Tr}\big(\big(\sigma_n^{\alpha_n}\mathcal{S}'\sigma_{n+1}^{\alpha_{n+1}} + \sigma_{n+1}^{\alpha_{n+1}}\mathcal{S}'\sigma_n^{\alpha_n}\big)\mathcal{S}\big). \quad (9)$$

With a chosen coupling (K_n, K_{n+1}) for the following time step, the quantum system is evolved accordingly, and the detector is measured subsequently. The stochastic outcome of this measurement is recorded and used to keep track of the running state on the classical computer.

We note that for the preparation of non-GHZ state families, one may choose a specific target value of the QFI, F_Q^*, and then minimize the cost function $|F_Q - F_Q^*|$. This approach allows one to use active steering protocols targeting different classes of state manifolds associated with a specific QFI value. As an example, we show results for Dicke states in Sec. III below.

III. NUMERICAL SIMULATION RESULTS

We now show simulation results for the above protocol maximizing the QFI. For the steering operator set (2), it is convenient to choose $\mathbf{s}_n = \frac{1}{\sqrt{2}}(1,0,1)^T$ [see Eq. (3)] but our results are robust under small rotations of this unit vector. Correspondingly, the GHZ states (1) are defined with respect to rotated states $|0\rangle \to |0'\rangle$ and $|1\rangle \to |1'\rangle$. Up to a normalization factor, $|0'\rangle = |0\rangle + (\sqrt{2}-1)|1\rangle$ and $|1'\rangle = (1-\sqrt{2})|0\rangle + |1\rangle$. In Fig. 2, we show the evolution of the time-dependent QFI. The main panel illustrates the average QFI $\overline{F_Q(t)}$ (the overbar indicates an average over many measurement trajectories) for several values of N, where we observe that the QFI comes closes to its maximum value $F_Q = N^2$ after $n_t \approx 200$ time steps. This number for n_t is basically independent of N. In the inset of Fig. 2, for $N = 5$, we illustrate the convergence behavior of the QFI both for individual measurement trajectories and for the average.

Next, we show that the target manifold (1) is reached to good accuracy. In Fig. 3(a), for $N = 5$, we show a histogram of the phase $\phi = \arg(\langle 0'0'0'\cdots|\Psi\rangle\langle\Psi|1'1'1'\cdots\rangle)$ measured after 500 time steps. We find that the histogram is rather flat, implying that the quantum state trajectories uniformly explore the entire manifold even though they all start from the same initial state. Alternatively, as illustrated in Fig. 3(b), one may take an individual measurement trajectory and follow it over time. For our choice of steering operators (2), almost regular oscillations are observed, where again all possible values of ϕ are reachable over the course of time. By invoking a termination policy, one can then target a specific state with a predesignated value of ϕ. Finally, in Fig. 3(c), we show the

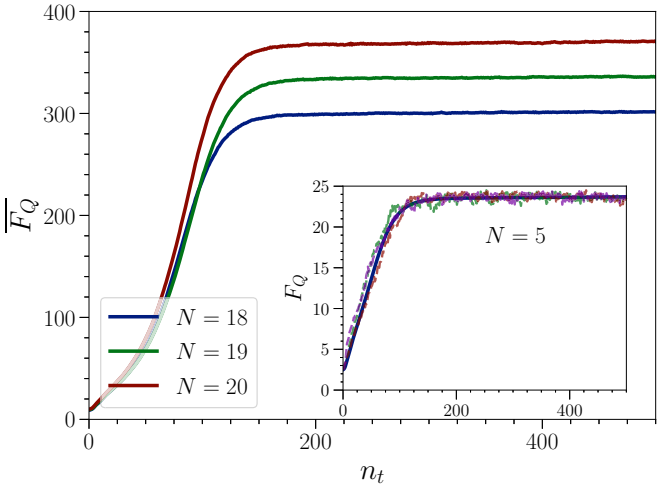


FIG. 2. Average QFI $\overline{F_Q}$ vs number of time steps $n_t = t/\delta t$ for different N and $J\delta t = 0.2$. Note that $F_Q \leqslant N^2$. Averages are over 100 trajectories. The inset shows $\overline{F_Q}$ vs n_t (solid curve) for $N = 5$ (averaged over 8000 trajectories), together with three individual measurement trajectories (dashed curves).

purity [48–50],

$$P(t) = \mathrm{Tr}(\overline{\rho(t)}^2), \quad (10)$$

as a function of n_t. Interestingly, the average state $\overline{\rho(t)}$ first approaches an infinite-temperature state where the purity gap (almost) closes [51], but the purity then increases again towards the asymptotic value 1/2. This value is readily explained by the fact that averaging over the phase in Eq. (1), one produces the asymptotic average state

$$\overline{\rho} = \tfrac{1}{2}(|000\cdots\rangle\langle 000\cdots| + |111\cdots\rangle\langle 111\cdots|), \quad (11)$$

which has purity $P = 1/2$ for all N. The difference to the numerically observed asymptotic purity in Fig. 3(c) is because of the finite value of $J\delta t$. We find that this difference becomes smaller by reducing $J\delta t$, see also below.

Let us now discuss the dependencies on the protocol's parameters. The scaling of the accuracy of the value of $\overline{F_Q}$ reached after $n_t = 500$ steps with system size N is shown in Fig. 4 for two values of $J\delta t$. We observe that for smaller $J\delta t$, higher accuracy can be reached because of the decreased importance of quantum jumps at long protocol times, which tend to deteriorate the QFI momentarily. However, using smaller values for $J\delta t$ comes with longer physical runtimes of the protocol.

In Fig. 5, we report the scaling of the number of steps n_t needed for reaching a QFI of $\overline{F_Q}/N^2 = 0.9$, for the same values of $J\delta t$ as in Fig. 4. Here, we also compare to a situation where one allows for Bell-pair measurements between arbitrary detector pairs (not only nearest neighbors) [see Fig. 1(c)], which tends to accelerate the protocol. In this case, all non-overlapping pairs (n, n') with $n, n' \in \{1, \ldots, N\}$ can again be steered simultaneously, where both the pairings (and the idle qubit for odd N) are chosen from a uniform random distribution for each time step. Such a fully connected Bell-measurement pairing scheme results in a faster

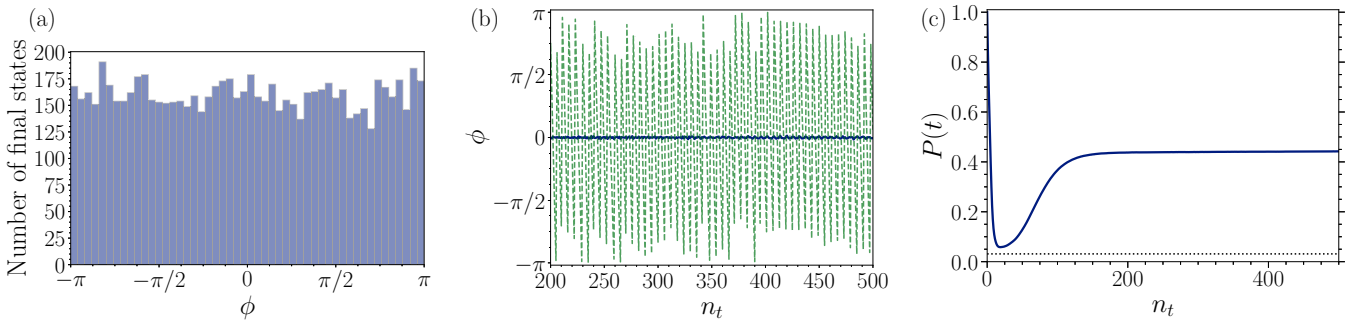


FIG. 3. Active steering protocol for $N = 5$ and $J\delta t = 0.2$. Measurement averages are over 8000 trajectories. (a) Histogram of the phase ϕ in Eq. (1) found after $n_t = 500$ time steps. (b) Time evolution of the phase ϕ after convergence to the target manifold has been reached, shown for one individual measurement trajectory (dashed-green curve) and for the average (solid-blue curve). (c) Purity $P(t)$ vs n_t; see Eq. (10). The dotted line corresponds to the maximally mixed (infinite temperature) state.

convergence to the target state since more options for finding optimal feedback Hamiltonians can be explored.

We observe an even-odd effect in Fig. 5, in particular for small N, which originates from the presence of the idle qubit for odd N in our Bell-pair measurement scheme. Remarkably, the required number of steps n_t increases only very slowly with N, suggesting *scalability* of the active steering protocol for large N. The fitting curves shown as thin solid lines in Fig. 5 indicate a scaling $n_t \sim \mathcal{O}(\ln N)$. Such favorable scaling is also corroborated by Fig. 2, where we show the n_t dependence of $\overline{F_Q}$ for several (large) values of N.

In addition to targeting states with maximum QFI, our protocol also allows for the preparation of states associated with different (nonmaximal) target values F_Q^* of the QFI. In order to do so, we simply choose $|F_Q - F_Q^*|$ as the cost function in the steering protocol. As an example of this approach, we here consider the case of *Dicke states* [19], which for qubits can be written as

$$|D_{k,N}\rangle = \binom{N}{k}^{-\frac{1}{2}} \sum_j \mathcal{P}_j (|0\rangle^{\otimes N-k} |1\rangle^{\otimes k}). \tag{12}$$

In Eq. (12), the sum runs over all possible permutations $\mathcal{P}_j$ of distributing k excited qubits in an N-qubit system. For the state in Eq. (12), the QFI has the value [19]

$$F_Q^* = \frac{N^2}{2} - 2\left(\frac{N}{2} - k\right)^2 + N. \tag{13}$$

As for GHZ states, the Dicke states in Eq. (12) can in addition contain arbitrary phase differences between the corresponding

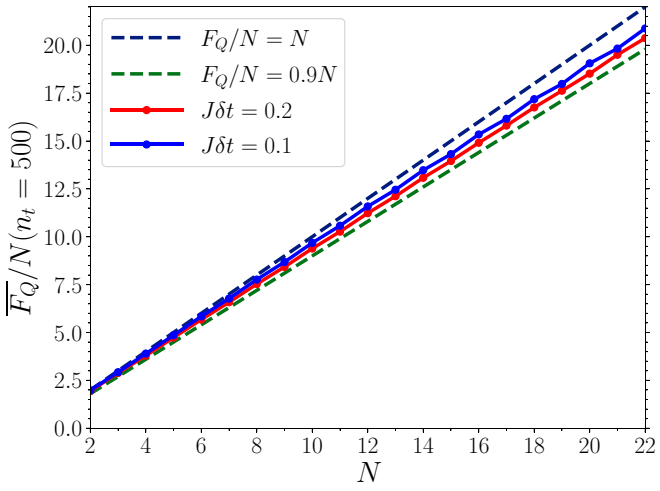


FIG. 4. Scaling of the accuracy of the asymptotic value of the averaged QFI $\overline{F_Q}/N$ vs N for $J\delta t = 0.1$ (blue) and $J\delta t = 0.2$ (red). Results have been averaged over at least 100 measurement trajectories. (For $N \leqslant 10$, we used 10000 trajectories; for $N = 11$ to 15, we averaged over 5000, and for $N \in \{16, 17\}$, over 1000 trajectories.) Solid lines are guides to the eye only. The upper bound, $\overline{F_Q}/N = N$, is shown as black-dashed line, the green-dashed line indicates $\overline{F_Q}/N = 0.9N$.

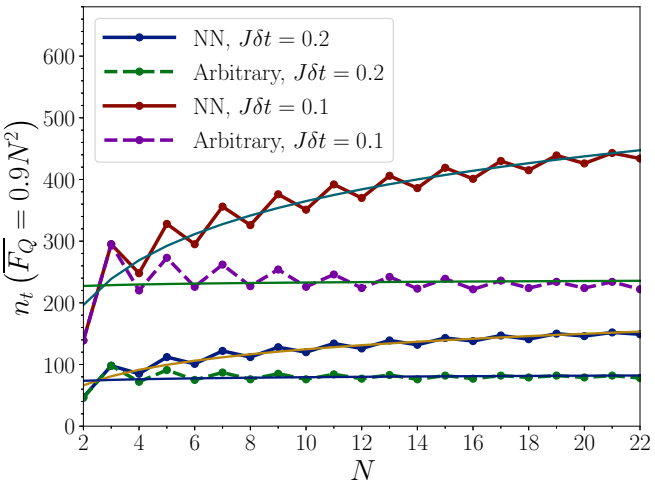


FIG. 5. Scaling of the step number n_t vs N needed for reaching the averaged QFI value $\overline{F_Q} = 0.9N^2$, shown for $J\delta t = 0.1$ and $J\delta t = 0.2$. Averages are over at least 100 trajectories. Thick-solid and dashed curves connecting data points are guides to the eye only. The thin-solid lines show numerical fits to the function $n_t^*(N) = A + B\ln(N)$ to the respective data, with fitting parameters A and B. For instance, we obtain $A \simeq 104.7$ and $B \simeq 123.9$ for nearest-neighbor couplings with $J\delta t = 0.1$ from such a fit. We show results for nearest-neighbor detector qubit measurements (solid) as well as allowing for arbitrary detector pair measurements (dashed curves); see Fig. 1.

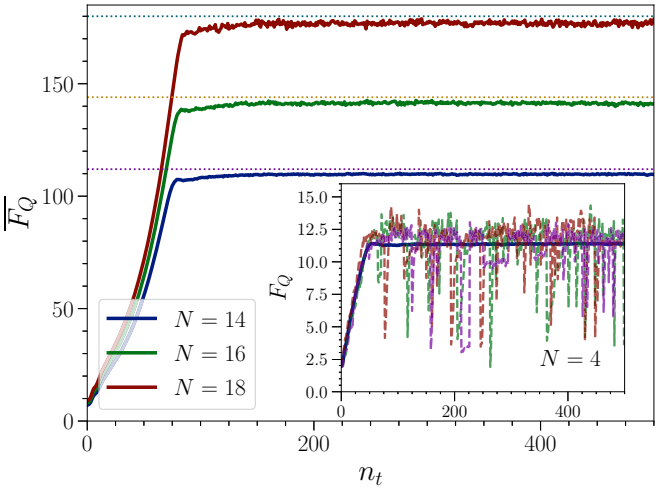


FIG. 6. Average QFI $\overline{F_Q}$ vs number of time steps $n_t = t/\delta t$ for an active steering protocol with cost function $|F_Q - F_Q^*|$ and F_Q^* in Eq. (13), targeting the Dicke states $|D_{k,N}\rangle$ in Eq. (12) for $k = N/2$ and various N, with $J\delta t = 0.2$. Averages are over 5000 (1000, 500) trajectories for $N = 14$ (16, 18). Dotted lines indicate the respective F_Q^* in Eq. (13). The inset shows $\overline{F_Q}$ vs n_t (solid curve, averaged over 10^4 trajectories) for $N = 4$, together with three individual measurement trajectories (dashed curves).

basis states, with the same value of F_Q^*. In general, our protocol will therefore target an entire state manifold for a given QFI value.

In analogy to Fig. 2, Fig. 6 shows numerical simulation results for the QFI-based preparation of Dicke states with the target value F_Q^* in Eq. (13) for $k = N/2$ and up to $N = 18$ qubits. We observe that the target value of the QFI is reached after $n_t \approx 70$ time steps, independently of the value of N. The protocol thus converges significantly faster than for GHZ states. However, even though $\overline{F_Q}$ is close to the target value F_Q^*, individual trajectories now exhibit stronger fluctuations; see the inset of Fig. 6. We note, in passing, that by implementing a stoppage criterion in the protocol [6], i.e., by terminating the protocol once the QFI target value has approximately been reached, we expect that such fluctuations can be reduced. In any case, we conclude that the QFI-based protocol is also useful for generating other highly entangled state manifolds beyond GHZ states.

IV. DISCUSSION

We have proposed an active steering protocol targeting the one-parameter manifold of N-qubit GHZ states (1) with genuine multipartite entanglement by means of weak Bell-pair measurements and active feedback. In contrast to fidelity-based cost functions [6], by using the QFI as a cost function, our results suggest that the active steering protocol may become scalable with increasing system size N. Although it is well known that GHZ states may be generated by projective measurements in shallow circuits [23,24,52], our results are relevant for at least two reasons beyond those specified in Sec. I: (i) We clarify similarities and differences between active and passive steering protocols for the case of a target state *manifold*. In passive steering [9,53], measurement outcomes are discarded. Such protocols are basically equivalent to driven-dissipative systems [54–58] with engineered dissipation; see Refs. [11,59–73] and corresponding experiments [31,74–78]. In contrast to the passive steering case, where the initial state uniquely determines the final state within the dark space forming the target manifold [79], we find that under active steering, the quantum state trajectory continues cycling through the target manifold. The initial state then plays no special role, and all phases ϕ in Eq. (1) are reached with equal probability as the protocol evolves. (ii) One may also target highly entangled nonstabilizer state manifolds, for which simpler routes along the lines of Ref. [52] are not available. Under quite general conditions, many highly entangled states, including Eq. (1), cannot be reached by driven-dissipative and/or passive steering [80]. For small N, it has been demonstrated that they remain accessible to active steering protocols [6].

In fact, one can apply a slightly modified version of the present protocol, which has favorable scaling properties with the system size, in order to prepare broad classes of other states, including the so-called W, Dicke, and cluster states [21]. This task may be achieved, for instance, by stopping the protocol at a suitable value of F_Q before convergence to the maximal QFI has been reached. Alternatively, one can select a target value F_Q^* for the QFI associated with the desired family of target states, and then choose $|F_Q - F_Q^*|$ as the cost function. For instance, the Dicke states $|D_{k,N}\rangle$ in Eq. (12) with associated QFI F_Q^* in Eq. (13) have been studied for $k = N/2$ excitations above; see Fig. 6. Another possibility to reach non-GHZ states is to add a nonstabilizerness quantifier [81,82] to the cost function.

For experiments, a modified implementation of our protocol where state tracking is not required would be highly beneficial. Without state tracking, one could both study larger system sizes and tolerate error channels with weak error rates. Such protocols can be formulated if weak measurements of all one- and two-body correlations present in the system state can be performed [11] since $\overline{dF_Q}$ in Eq. (6) depends only on those correlations. As a result, the protocol could be entirely based on the outcomes of weak measurements without any need for state tracking. In particular, our simulations only use the values of the one- and two-body correlations R_{μ_i} and $Q_{n,m}^{\alpha_n,\alpha_m}$ defined after Eq. (8) in order to determine the optimal couplings K entering the feedback Hamiltonian. Counting the number of one- and two-body correlators, we expect that the performance of such a protocol will scale $\sim N^2$. Noting that our numerical simulations are mainly limited by the computational demands of updating the SSE, which is not necessary when switching to a protocol directly utilizing weak measurements of one- and two-body correlations, we expect that such a protocol can be applied to larger values of N. In addition, it allows for the presence of error channels and/or measurement inefficiencies. However, a detailed exploration of this interesting direction is beyond the scope of this paper.

Finally, given that the state manifolds our protocol can target could allow one to overcome classical limits in quantum phase estimation and to attain the so-called Heisenberg limit [16–18,20], it is a promising option to employ active steering protocols using the QFI for entanglement-enhanced metrology and sensing applications; see also

Refs. [19,83–85]. However, this remains feasible provided errors have a limited impact and that an optimal measurement, dependent on the state, can be performed. A comprehensive analysis of how errors affect state preparation, sensing, and measurement is left for future work.

ACKNOWLEDGMENTS

We thank S. Diehl, Y. Gefen, and I. Gornyi for discussions. We acknowledge funding by the Deutsche Forschungsgemeinschaft (DFG, German Research Foundation) under Project No. 277101999 - TRR 183 (Project No. B02), and under Germany's Excellence Strategy - Cluster of Excellence Matter and Light for Quantum Computing (ML4Q) EXC 2004/1 - 390534769.

DATA AVAILABILITY

The data that support the findings of this article are openly available [86,87].

[1] V. V. Sivak, A. Eickbusch, H. Liu, B. Royer, I. Tsioutsios, and M. H. Devoret, Model-free quantum control with reinforcement learning, Phys. Rev. X **12**, 011059 (2022).
[2] Q. Liu, K. Ziegler, D. A. Kessler, and E. Barkai, Driving quantum systems with periodic conditional measurements, Phys. Rev. Res. **4**, 023129 (2022).
[3] A. J. Friedman, O. Hart, and R. Nandkishore, Measurement-induced phases of matter require feedback, PRX Quantum **4**, 040309 (2023).
[4] Y. Herasymenko, I. Gornyi, and Y. Gefen, Measurement-driven navigation in many-body Hilbert space: Active-decision steering, PRX Quantum **4**, 020347 (2023).
[5] V. Ravindranath, Y. Han, Z.-C. Yang, and X. Chen, Entanglement steering in adaptive circuits with feedback, Phys. Rev. B **108**, L041103 (2023).
[6] S. Morales, Y. Gefen, I. Gornyi, A. Zazunov, and R. Egger, Engineering unsteerable quantum states with active feedback, Phys. Rev. Res. **6**, 013244 (2024).
[7] J. Hauser, Y. Li, S. Vijay, and M. P. A. Fisher, Continuous symmetry breaking in adaptive quantum dynamics, Phys. Rev. B **109**, 214305 (2024).
[8] N. Ackermann, S. Morales, A. L. Yeyati, S. Diehl, and R. Egger, Error threshold in active steering protocols for few-qubit systems, Phys. Rev. Res. **7**, 013045 (2025).
[9] S. Roy, J. T. Chalker, I. V. Gornyi, and Y. Gefen, Measurement-induced steering of quantum systems, Phys. Rev. Res. **2**, 033347 (2020).
[10] R. Uola, A. C. S. Costa, H. C. Nguyen, and O. Gühne, Quantum steering, Rev. Mod. Phys. **92**, 015001 (2020).
[11] H. M. Wiseman and G. J. Milburn, *Quantum Measurements and Control* (Cambridge University Press, Cambridge, 2010).
[12] C. W. Helstrom, Quantum detection and estimation theory, J. Stat. Phys. **1**, 231 (1969).
[13] V. Giovannetti, S. Lloyd, and L. Maccone, Advances in quantum metrology, Nat. Photon. **5**, 222 (2011).
[14] P. Hyllus, W. Laskowski, R. Krischek, C. Schwemmer, W. Wieczorek, H. Weinfurter, L. Pezzé, and A. Smerzi, Fisher information and multiparticle entanglement, Phys. Rev. A **85**, 022321 (2012).
[15] G. Tóth, Multipartite entanglement and high-precision metrology, Phys. Rev. A **85**, 022322 (2012).
[16] M. G. Paris, Quantum estimation for quantum technology, Int. J. Quantum Inf. **07**, 125 (2009).
[17] L. Pezzé and A. Smerzi, Entanglement, nonlinear dynamics, and the Heisenberg limit, Phys. Rev. Lett. **102**, 100401 (2009).
[18] G. Tóth and I. Apellaniz, Quantum metrology from a quantum information science perspective, J. Phys. A: Math. Theor. **47**, 424006 (2014).
[19] L. Pezzè, A. Smerzi, M. K. Oberthaler, R. Schmied, and P. Treutlein, Quantum metrology with nonclassical states of atomic ensembles, Rev. Mod. Phys. **90**, 035005 (2018).
[20] J. Liu, H. Yuan, X.-M. Lu, and X. Wang, Quantum Fisher information matrix and multiparameter estimation, J. Phys. A: Math. Theor. **53**, 023001 (2019).
[21] M. A. Nielsen and I. L. Chuang, *Quantum Computation and Quantum Information* (Cambridge University Press, Cambridge, 2000).
[22] E. H. Chen, G.-Y. Zhu, R. Verresen, A. Seif, E. Bäumer, D. Layden, N. Tantivasadakarn, G. Zhu, S. Sheldon, A. Vishwanath, S. Trebst, and A. Kandala, Nishimori transition across the error threshold for constant-depth quantum circuits, Nat. Phys. **21**, 161 (2025).
[23] R. Sahay and R. Verresen, Classifying one-dimensional quantum states prepared by a single round of measurements, PRX Quantum **6**, 010329 (2025).
[24] R. Sahay and R. Verresen, Finite-depth preparation of tensor network states from measurement, arXiv:2404.17087.
[25] O. Hosten and P. Kwiat, Observation of the spin Hall effect of light via weak measurements, Science **319**, 787 (2008).
[26] P. B. Dixon, D. J. Starling, A. N. Jordan, and J. C. Howell, Ultrasensitive beam deflection measurement via interferometric weak value amplification, Phys. Rev. Lett. **102**, 173601 (2009).
[27] A. Palacios-Laloy, F. Mallet, F. Nguyen, P. Bertet, D. Vion, D. Esteve, and A. N. Korotkov, Experimental violation of a Bell's inequality in time with weak measurement, Nat. Phys. **6**, 442 (2010).
[28] D. Riste, M. Dukalski, C. A. Watson, G. de Lange, M. J. Tiggelman, Y. M. Blanter, K. W. Lehnert, R. N. Schouten, and L. DiCarlo, Deterministic entanglement of superconducting qubits by parity measurement and feedback, Nature (London) **502**, 350 (2013).
[29] J. P. Groen, D. Ristè, L. Tornberg, J. Cramer, P. C. de Groot, T. Picot, G. Johansson, and L. DiCarlo, Partial-measurement backaction and nonclassical weak values in a superconducting circuit, Phys. Rev. Lett. **111**, 090506 (2013).
[30] J. Zhang, Y. Liu, R.-B. Wu, K. Jacobs, and F. Nori, Quantum feedback: Theory, experiments, and applications, Phys. Rep. **679**, 1 (2017).
[31] Z. K. Minev, S. O. Mundhada, S. Shankar, P. Reinhold, R. Gutiérrez-Jáuregui, R. J. Schoelkopf, M. Mirrahimi,

H. J. Carmichael, and M. H. Devoret, To catch and reverse a quantum jump mid-flight, Nature (London) **570**, 200 (2019).
[32] K. S. Cujia, J. M. Boss, K. Herb, J. Zopes, and C. L. Degen, Tracking the precession of single nuclear spins by weak measurements, Nature (London) **571**, 230 (2019).
[33] Y. Kim, D.-G. Im, Y.-S. Kim, S.-W. Han, S. Moon, Y.-H. Kim, and Y.-W. Cho, Observing the quantum Cheshire cat effect with noninvasive weak measurement, npj Quantum Inf. **7**, 13 (2021).
[34] K. Jacobs and D. A. Steck, A straightforward introduction to continuous quantum measurement, Contemp. Phys. **47**, 279 (2006).
[35] C. Janvier, L. Tosi, L. Bretheau, Ç. Ö. Girit, M. Stern, P. Bertet, P. Joyez, D. Vion, D. Esteve, M. F. Goffman *et al.*, Coherent manipulation of Andreev states in superconducting atomic contacts, Science **349**, 1199 (2015).
[36] M. Pita-Vidal, J. J. Wesdorp, and C. K. Andersen, Blueprint for all-to-all-connected superconducting spin qubits, PRX Quantum **6**, 010308 (2025).
[37] D. Volya and P. Mishra, Quantum steering of surface error correcting codes, in *2023 IEEE International Conference on Quantum Computing and Engineering (QCE)* (Bellevue, Washington, USA, 2023), Vol. 01, p. 1394.
[38] D. Volya and P. Mishra, FL state preparation on quantum computers via quantum steering, IEEE Trans. Quantum Eng. **5**1 (2024).
[39] D. Boschi, S. Branca, F. De Martini, L. Hardy, and S. Popescu, Experimental realization of teleporting an unknown pure quantum state via dual classical and Einstein-Podolsky-Rosen channels, Phys. Rev. Lett. **80**, 1121 (1998).
[40] J.-W. Pan, D. Bouwmeester, H. Weinfurter, and A. Zeilinger, Experimental entanglement swapping: Entangling photons that never interacted, Phys. Rev. Lett. **80**, 3891 (1998).
[41] T. Jennewein, G. Weihs, J.-W. Pan, and A. Zeilinger, Experimental nonlocality proof of quantum teleportation and entanglement swapping, Phys. Rev. Lett. **88**, 017903 (2001).
[42] H. de Riedmatten, I. Marcikic, J. A. W. van Houwelingen, W. Tittel, H. Zbinden, and N. Gisin, Long-distance entanglement swapping with photons from separated sources, Phys. Rev. A **71**, 050302(R) (2005).
[43] M. Riebe, T. Monz, K. Kim, A. S. Villar, P. Schindler, M. Chwalla, M. Hennrich, and R. Blatt, Deterministic entanglement swapping with an ion-trap quantum computer, Nat. Phys. **4**, 839 (2008).
[44] R. Kaltenbaek, R. Prevedel, M. Aspelmeyer, and A. Zeilinger, High-fidelity entanglement swapping with fully independent sources, Phys. Rev. A **79**, 040302(R) (2009).
[45] R. Horodecki, P. Horodecki, M. Horodecki, and K. Horodecki, Quantum entanglement, Rev. Mod. Phys. **81**, 865 (2009).
[46] C.-X. Huang, X.-M. Hu, Y. Guo, C. Zhang, B.-H. Liu, Y.-F. Huang, C.-F. Li, G.-C. Guo, N. Gisin, C. Branciard, and A. Tavakoli, Entanglement swapping and quantum correlations via symmetric joint measurements, Phys. Rev. Lett. **129**, 030502 (2022).
[47] H. P. Breuer and F. Petruccione, *The Theory of Open Quantum Systems* (Oxford University Press, Oxford, 2002).
[48] B. Schumacher and M. A. Nielsen, Quantum data processing and error correction, Phys. Rev. A **54**, 2629 (1996).
[49] S. Lloyd, Capacity of the noisy quantum channel, Phys. Rev. A **55**, 1613 (1997).
[50] R. Fan, Y. Bao, E. Altman, and A. Vishwanath, Diagnostics of mixed-state topological order and breakdown of quantum memory, PRX Quantum **5**, 020343 (2024).
[51] M. Buchhold, Y. Minoguchi, A. Altland, and S. Diehl, Effective theory for the measurement-induced phase transition of Dirac fermions, Phys. Rev. X **11**, 041004 (2021).
[52] J. F. Kam, H. Kang, C. D. Hill, G. J. Mooney, and L. C. L. Hollenberg, Characterization of entanglement on superconducting quantum computers of up to 414 qubits, Phys. Rev. Res. **6**, 033155 (2024).
[53] E. Medina-Guerra, P. Kumar, I. V. Gornyi, and Y. Gefen, Quantum state engineering by steering in the presence of errors, Phys. Rev. Res. **6**, 023159 (2024).
[54] J. F. Poyatos, J. I. Cirac, and P. Zoller, Quantum reservoir engineering with laser cooled trapped ions, Phys. Rev. Lett. **77**, 4728 (1996).
[55] S. Diehl, A. Micheli, A. Kantian, B. Kraus, H. P. Büchler, and P. Zoller, Quantum states and phases in driven open quantum systems with cold atoms, Nat. Phys. **4**, 878 (2008).
[56] F. Verstraete, M. Wolf, and J. Ignacio Cirac, Quantum computation and quantum-state engineering driven by dissipation, Nat. Phys. **5**, 633 (2009).
[57] J. T. Barreiro, M. Müller, P. Schindler, D. Nigg, T. Monz, M. Chwalla, M. Hennrich, C. F. Roos, P. Zoller, and R. Blatt, An open-system quantum simulator with trapped ions, Nature (London) **470**, 486 (2011).
[58] H. Krauter, C. A. Muschik, K. Jensen, W. Wasilewski, J. M. Petersen, J. I. Cirac, and E. S. Polzik, Entanglement generated by dissipation and steady state entanglement of two macroscopic objects, Phys. Rev. Lett. **107**, 080503 (2011).
[59] J. P. Paz and W. H. Zurek, Continuous error correction, Proc. R. Soc. London, Ser. A **454**, 355 (1998).
[60] J. P. Barnes and W. S. Warren, Automatic quantum error correction, Phys. Rev. Lett. **85**, 856 (2000).
[61] C. Ahn, A. C. Doherty, and A. J. Landahl, Continuous quantum error correction via quantum feedback control, Phys. Rev. A **65**, 042301 (2002).
[62] C. Ahn, H. M. Wiseman, and G. J. Milburn, Quantum error correction for continuously detected errors, Phys. Rev. A **67**, 052310 (2003).
[63] M. Sarovar, C. Ahn, K. Jacobs, and G. J. Milburn, Practical scheme for error control using feedback, Phys. Rev. A **69**, 052324 (2004).
[64] O. Oreshkov and T. A. Brun, Continuous quantum error correction for non-Markovian decoherence, Phys. Rev. A **76**, 022318 (2007).
[65] J. Kerckhoff, H. I. Nurdin, D. S. Pavlichin, and H. Mabuchi, Designing quantum memories with embedded control: Photonic circuits for autonomous quantum error correction, Phys. Rev. Lett. **105**, 040502 (2010).
[66] E. Kapit, Hardware-efficient and fully autonomous quantum error correction in superconducting circuits, Phys. Rev. Lett. **116**, 150501 (2016).
[67] E. Kapit, Error-transparent quantum gates for small logical qubit architectures, Phys. Rev. Lett. **120**, 050503 (2018).
[68] M. Gau, R. Egger, A. Zazunov, and Y. Gefen, Driven dissipative Majorana dark spaces, Phys. Rev. Lett. **125**, 147701 (2020).
[69] M. Gau, R. Egger, A. Zazunov, and Y. Gefen, Towards dark space stabilization and manipulation in driven dissipative Majorana platforms, Phys. Rev. B **102**, 134501 (2020).

[70] S. Lieu, R. Belyansky, J. T. Young, R. Lundgren, V. V. Albert, and A. V. Gorshkov, Symmetry breaking and error correction in open quantum systems, Phys. Rev. Lett. **125**, 240405 (2020).

[71] S. Lieu, Y.-J. Liu, and A. V. Gorshkov, Candidate for a passively protected quantum memory in two dimensions, Phys. Rev. Lett. **133**, 030601 (2024).

[72] O. Shtanko, Y.-J. Liu, S. Lieu, A. V. Gorshkov, and V. V. Albert, Bounds on autonomous quantum error correction, arXiv:2308.16233.

[73] L. B. Kristensen, M. Kjaergaard, C. K. Andersen, and N. T. Zinner, Hybrid quantum error correction in qubit architectures, Phys. Rev. A **108**, 022403 (2023).

[74] Z. Leghtas, U. Vool, S. Shankar, M. Hatridge, S. M. Girvin, M. H. Devoret, and M. Mirrahimi, Stabilizing a Bell state of two superconducting qubits by dissipation engineering, Phys. Rev. A **88**, 023849 (2013).

[75] P. Campagne-Ibarcq, A. Eickbusch, S. Touzard, E. Zalys-Geller, N. E. Frattini, V. V. Sivak, P. Reinhold, S. Puri, S. Shankar, R. J. Schoelkopf *et al.*, Quantum error correction of a qubit encoded in grid states of an oscillator, Nature (London) **584**, 368 (2020).

[76] J. M. Gertler, B. Baker, J. Li, S. Shirol, J. Koch, and C. Wang, Protecting a bosonic qubit with autonomous quantum error correction, Nature (London) **590**, 243 (2021).

[77] W. P. Livingston, M. S. Blok, E. Flurin, J. Dressel, A. N. Jordan, and I. Siddiqi, Experimental demonstration of continuous quantum error correction, Nat. Commun. **13**, 2307 (2022).

[78] D. Lachance-Quirion, M.-A. Lemonde, J. O. Simoneau, L. St-Jean, P. Lemieux, S. Turcotte, W. Wright, A. Lacroix, J. Fréchette-Viens, R. Shillito, F. Hopfmueller, M. Tremblay, N. E. Frattini, J. Camirand Lemyre, and P. St-Jean, Autonomous quantum error correction of Gottesman-Kitaev-Preskill states, Phys. Rev. Lett. **132**, 150607 (2024).

[79] P. Zanardi and L. Campos Venuti, Coherent quantum dynamics in steady-state manifolds of strongly dissipative systems, Phys. Rev. Lett. **113**, 240406 (2014).

[80] F. Ticozzi and L. Viola, Stabilizing entangled states with quasi-local quantum dynamical semigroups, Philos. Trans. R. Soc. A **370**, 5259 (2012).

[81] A. Ahmadi and E. Greplova, Quantifying non-stabilizerness via information scrambling, SciPost Phys. **16**, 043 (2024).

[82] P. S. Tarabunga, M. Frau, T. Haug, E. Tirrito, and L. Piroli, A nonstabilizerness monotone from stabilizerness asymmetry, arXiv:2411.05766.

[83] E. Davis, G. Bentsen, and M. Schleier-Smith, Approaching the Heisenberg limit without single-particle detection, Phys. Rev. Lett. **116**, 053601 (2016).

[84] T. Macrì, A. Smerzi, and L. Pezzè, Loschmidt echo for quantum metrology, Phys. Rev. A **94**, 010102(R) (2016).

[85] S. Dooley, S. Pappalardi, and J. Goold, Entanglement enhanced metrology with quantum many-body scars, Phys. Rev. B **107**, 035123 (2023).

[86] S. Morales, S. Pappalardi, and R. Egger, Data for "Towards scalable active steering protocols for genuinely entangled state manifods", [Data Set] Zenodo (2025), doi: 10.5281/zenodo.14277545.

[87] S. Morales, S. Pappalardi, and R. Egger, Code for "Towards scalable active steering protocols for genuinely entangled state manifods" (2025), https://github.com/Sammor13/QFI_steering.